

High-resolution observations of water masers in Bok globules

Itziar de Gregorio-Monsalvo¹, José F. Gómez², Olga Suárez¹, Thomas B. H. Kuiper³,
Guillem Anglada², Nimesh A. Patel⁴, José M. Torrelles⁵

ABSTRACT

We present Very Large Array observations at 1.3 cm of several water maser detections obtained by previous single-dish studies of Bok globules in the Clemens & Barvainis (1988; CB) catalog. We report water maser emission in CB 3 (CB3-mm), CB 54 (IRAS 07020–1618), CB 101 (IRAS 17503–0833), and CB 232 (IRAS 21352+4307), and non-detection towards CB 65 (IRAS 16277–2332) and CB 205 (IRAS 19433+2743). These are the first reported interferometric observations of water masers in Bok globules of the CB catalog. We also present single-dish observations of millimeter and centimeter spectral lines towards CB 101 (IRAS 17503–0833) and CB 65 (IRAS 16277–2332). All the maser emission seems to be associated with star forming regions hosting bipolar molecular outflows, except IRAS 17503–0833 in CB 101, which we suggest to be a possible Mira evolved star, and IRAS 16277–2332 in CB 65, of unknown nature. We have used the precise position of the maser emission to derive information about the powering source of the masers. By analyzing the spatio-kinematical distribution of the water masers, we confirm the millimeter source CB 3-mm as the most likely powering source of the CB 3 masers. We propose the near-IR source CB 232 YC1-I as the best candidate for pumping the maser emission observed in CB

¹Laboratorio de Astrofísica Espacial y Física Fundamental (INTA), Apartado 50727, E-28080 Madrid, Spain; itziar@laeff.inta.es, olga@laeff.inta.es

²Instituto de Astrofísica de Andalucía (CSIC), Apartado 3004, E-18080 Granada, Spain; jfg@iaa.es, guillem@iaa.es.

³Jet Propulsion Laboratory, California Institute of Technology, 4800 Oak Grove Drive, Pasadena, CA 91109, USA; kuiper@jpl.nasa.gov.

⁴Harvard-Smithsonian Center for Astrophysics, 60 Garden Street, Cambridge, MA 02138, USA; npatel@cfa.harvard.edu.

⁵Instituto de Ciencias del Espacio (CSIC) and Institut d'Estudis Espacials de Catalunya, Facultat de Física, Planta 7, Universitat de Barcelona, Av. Diagonal 647, E-08028 Barcelona, Spain; torrelles@ieec.fcr.es.

232, while in CB 54, we suggest that the pumping source of the masers could be located at the position of an elongated feature observed in near-infrared maps.

Subject headings: masers—radio continuum: ISM—stars: pre-main sequence—ISM: globules, jets and outflows, molecules.

1. Introduction

Bok globules (Bok & Reilly 1947) are small ($\lesssim 1$ pc), isolated clouds, some of which are sites of low- and intermediate-mass star formation (Yun & Clemens 1990). They have been observed to be in different evolutionary stages, from starless dark cores (Yun et al. 1996; Kane & Clemens 1997) to sites hosting T-Tauri stars (Yun & Clemens 1995; Launhardt & Henning 1997). These globules have traditionally been considered important laboratories for the study of star formation processes, since their small size and relative simplicity make these processes less likely to be affected by confusion from different generations of young stellar objects. Another important aspect of star formation in Bok globules is that it may explain the somewhat puzzling existence of pre-main-sequence objects apparently not related with known molecular clouds. At least some of these objects may have originated in already dispersed Bok globules (Launhardt & Henning 1997).

Among the observational tools used in star-formation studies, water masers have proved to be a very powerful one. Water maser emission at 22 GHz is a good tracer of mass-loss activity in young stars (Rodríguez et al. 1980; Felli et al. 1992; Xiang & Turner 1995; De Buizer et al. 2005). In the low-mass young stellar objects (YSOs) this signpost of mass loss phenomena occurs in their most embedded phase, at the earliest stages of evolution. This period is characterized by the presence of the disk/young stellar object/outflow system (Shu et al. 1987) and a large amount of circumstellar dust. In the low-mass YSOs framework, the youngest evolutionary stage is represented by Class 0 sources (André et al. 1993), which show the most powerful and collimated molecular outflows (e.g., Hirano et al. 2006, and references therein), centimeter emission (e.g. Anglada 1995), and host strong submillimeter and millimeter continuum emission (André et al. 1993; André & Montmerle 1994).

Water maser studies have shown that this emission provides a good characterization of the age of low-mass YSOs (e.g. Furuya et al. 2001), with Class 0 sources being the most probable candidates to harbor water maser emission, due to the interaction of powerful jets with a larger amount of circumstellar material. This fact makes sources that host water maser emission good candidates for being in a very early stage of its evolution. In addition, several water maser surveys towards low-mass YSOs have shown that this emission tends to

be located close (within several hundred AU) to the central powering source (Chernin 1995; Claussen et al. 1998; Furuya et al. 2000, 2003). These characteristics make the water maser phenomenon well-suited to derive information about the location of the exciting source of the mass-loss phenomena observed in young star forming regions. Moreover, maser emission can be a useful tool for studying the physical conditions and kinematics of the gas surrounding the most embedded YSOs at very high angular resolution (≤ 1 mas), due to the very specific conditions which pump the maser emission (hundreds of K and $n_{\text{H}_2} \simeq 10^8 - 10^{10} \text{ cm}^{-3}$) (Claussen et al. 1998; Furuya et al. 2000; Patel et al. 2000; Torrelles et al. 2003; Goddi et al. 2005; Marvel 2005; Vlemmings et al. 2006). These conditions can be generated in shocked gas compressed by winds (Chernin 1995; Torrelles et al. 1997; Furuya et al. 2000; Moscadelli et al. 2000), as well as in circumstellar disks (Fiebig et al. 1996; Torrelles et al. 1996, 1998; Seth et al. 2002; Brand et al. 2003). This dichotomy has also been suggested to be a possible evolutionary sequence, with water masers tracing gravitationally bound material (e.g., circumstellar disks) in the youngest sources, and outflows in more evolved YSOs (Torrelles et al. 1997, 1998). Recently, the hot dense infalling gas after the accretion shock has also been proposed as a good environment for pumping the maser emission (Menten & van der Tak 2004).

Therefore, there are different evolutionary aspects related to water maser emission (e.g., the likely occurrence of masers in Class 0 YSOs, and their association with either disks and jets). Bok globules are appropriate sites to study evolution of YSOs, since they are usually identified as dark patches in optical images, without any selection criterion related to possible star-forming activity (Clemens & Barvainis 1988, hereafter CB; Bourke et al. 1995), and therefore they may span a large range of evolutionary stages. Surprisingly, studies of water masers in Bok globules are relatively scarce. Recently, our group undertook a sensitive and systematic single-dish survey for water masers in 207 positions within Bok globules (Gómez et al. 2006), using NASA’s 70m antenna in Robledo de Chavela (Spain), which provided six new detections in CB 34, CB 54, CB 65, CB 101, CB 199, and CB 232. Before this survey, only Scappini et al. (1991) conducted a search for water masers specifically in Bok globules, with 80 target positions and only one detection towards CB 3. Other surveys for water masers included some Bok globules within their target positions (e.g., Felli et al. 1992; Palla & Prusti 1993; Wouterloot et al. 1993; Persi et al. 1994; Codella et al. 1995), although they did not find any detection in these types of sources.

Using as a reference the catalogs of Bok globules of CB in the northern hemisphere, and Bourke et al. (1995) in the southern one (probably the more complete ones available), we are only aware of 9 Bok globules in those catalogs that are apparently associated with water maser emission: The six new detections mentioned above in the survey by Gómez et al. (2006), the detection towards CB 3 reported by Scappini et al. (1991), as well as

the detections obtained by Schwartz & Buhl (1975) and Neckel et al. (1985) in CB 39 and CB 205 respectively. All these reported detections of masers in Bok globules present single-dish data. However, interferometric high-angular resolution observations are necessary to pinpoint accurately the actual pumping source of water maser emission among several candidates, and to determine whether maser emission in these Bok globules tends to trace collimated jets or circumstellar disks.

In this paper we present for the first time interferometric, high-angular resolution observations using the Very Large Array (VLA) of the National Radio Astronomy Observatory¹ of some of these water masers in Bok globules. This paper is structured as follows: in §2 we describe our observations and data processing; in §3 we present our observational results and we discuss them; we summarize our conclusions in §4.

2. Observations and data processing

2.1. Target selection

We present interferometric observations using the VLA in the Bok globules in which water masers were detected in the survey by Gómez et al. (2006) between 2002 April and 2003 May (i.e., CB 54, CB 65, CB 101, and CB 232), as well as CB 3 (Scappini et al. 1991) and CB 205 (Neckel et al. 1985). The interferometric data have been complemented with a multimolecular single-dish study at millimeter and centimeter wavelengths using the IRAM-30m and Robledo-70m antenna of CB 101 (IRAS 17503–0833) and CB 65 (IRAS 16277–2332), in order to better understand the nature of these sources, and determine the internal structure of their surrounding region.

2.2. VLA Observations

We observed simultaneously the $6_{16}-5_{23}$ transition of H_2O (rest frequency = 22235.080 MHz) and continuum at 1.3 cm with the VLA, toward the Bok globules CB 54, CB 65, CB 101, CB 205, and CB 232. The observations were carried out on 2004 February 2 and 3 using the VLA in its CnB configuration, except for the CB 65 observations that were carried out on 2005 February 12 in the BnA configuration. We selected the four IF spectral

¹The National Radio Astronomy Observatory is a facility of the National Science Foundation operated under cooperative agreement by Associated Universities, Inc.

line mode to observe line and continuum simultaneously, processing both right and left circular polarizations, which we averaged together. Two IFs were used to observe the water maser transition, sampled on 64 channels over a bandwidth of 3.125 MHz, with a velocity resolution of 0.66 km s^{-1} . The other two IFs were used for radio continuum observations at 1.3 cm, covering a 25 MHz bandwidth on 8 channels, and centered 50 MHz above the central frequency used for line observations. The central velocity of the bands for line observations, the coordinates of the phase centers and the synthesized beam information are listed in Table 1 for each source. The primary calibrators were 3C48 (adopted flux density of 1.132 Jy) for observations on 2004 February 2, and 3C286 (adopted flux density of 2.539 Jy) for observations on 2004 February 3 and 2005 February 12. The phase calibrators and their bootstrapped flux densities are given in Table 1. We used J0609-157, J1743-038, and 3C286 as bandpass calibrators. Calibration and data reduction were performed with the Astronomical Image Processing System (AIPS) of NRAO. We detected water maser emission in CB 54, CB 101, and CB 232 (see Table 2), but we did not detect any emission towards either CB 65 or CB 205. In the case of CB 101 and CB 232, maser data were self-calibrated, and spectral Hanning smoothing was applied (to alleviate ringing in the bandpass), which provides a final velocity resolution of $\sim 1.3 \text{ km s}^{-1}$. The continuum data of these two sources were cross-calibrated using the self-calibration solutions obtained for the stronger maser lines. None of the sources is detected in radio continuum (see §3), probably because the typical values of the centimeter continuum emission observed in Bok globules (see Moreira et al. 1997, 1999) fall below our sensitivity limit

We have also processed water maser data in source CB 3, taken from the VLA archive. The observations were carried out on 1995 October 28, in the B configuration. These observations were made in the IIF spectral line mode, in right circular polarization only, with a bandwidth of 6.25 MHz sampled over 128 channels (velocity resolution of 0.66 km s^{-1}). The velocity of the center of the bandwidth, coordinates of the phase center, and synthesized beam size are also listed in Table 1. The source 3C48 was used as primary flux calibrator, with an assumed flux density of 1.131 Jy, while J0136+478 was used as phase and bandpass calibrator (Table 1). Water maser emission was detected toward CB 3 (see Table 2). The data were self-calibrated and spectral Hanning smoothing was applied, with a final velocity resolution of $\sim 1.3 \text{ km s}^{-1}$.

2.3. Single-dish observations

2.3.1. IRAM 30 m

Millimeter single-dish observations were carried out towards CB 65 (IRAS 16277–2332) and CB 101 (IRAS 17503–0833) with the IRAM 30-m telescope at Pico Veleta (Spain), in 2004 July-August. We have used Superconductor-Insulator-Superconductor (SIS) heterodyne receivers to observe nine different transitions at ~ 1.3 , ~ 2.7 , and ~ 3 mm. We observed the $^{13}\text{CO}(J = 1 \rightarrow 0)$, $^{13}\text{CO}(J = 2 \rightarrow 1)$, $\text{C}^{18}\text{O}(J = 1 \rightarrow 0)$, $\text{C}^{18}\text{O}(J = 2 \rightarrow 1)$, $\text{CO}(J = 1 \rightarrow 0)$, $\text{CO}(J = 2 \rightarrow 1)$, $\text{SiO}(J = 2 \rightarrow 1)$, $\text{CS}(J = 2 \rightarrow 1)$, and $\text{CS}(J = 5 \rightarrow 4)$ lines towards CB 101. In the case of CB 65, only the $\text{CO}(J = 1 \rightarrow 0)$ and $\text{CO}(J = 2 \rightarrow 1)$ lines were observed. In Table 3 we have summarized the rest frequencies of the different molecular transitions observed, the typical system temperature (T_{sys}), the half power beam width, the main beam efficiency, averaging area in case the spectrum corresponds to the average of several positions, and the derived line parameters. Pointing was checked every hour by observing J1743–038, giving a pointing accuracy better than $2''$. The observations were made by wobbling the secondary mirror to a distance of $220''$ from the source for $\text{CO}(J = 1 \rightarrow 0)$, $\text{CO}(J = 2 \rightarrow 1)$, and $\text{CS}(J = 5 \rightarrow 4)$ transitions, and in frequency switching mode for $\text{C}^{18}\text{O}(J = 1 \rightarrow 0)$, $\text{C}^{18}\text{O}(J = 2 \rightarrow 1)$, $^{13}\text{CO}(J = 1 \rightarrow 0)$, $^{13}\text{CO}(J = 2 \rightarrow 1)$, $\text{CS}(J = 2 \rightarrow 1)$, and $\text{SiO}(J = 2 \rightarrow 1)$ transitions. In addition, we observed $\text{CO}(J = 1 \rightarrow 0)$ and $\text{CO}(J = 2 \rightarrow 1)$ in frequency switching mode at one selected position to better estimate the excitation conditions. The data were taken with the versatile spectrometer assembly (VESPA) autocorrelator, split into two or three parts (depending on the lines), to observe simultaneously two or three different frequencies. This provided resolutions between 0.05 and 0.4 km s^{-1} at 1.3 mm, between 0.05 and 0.8 km s^{-1} at 2.7 mm, and $\simeq 0.06 \text{ km s}^{-1}$ at 3 mm. Moreover, we used a 1 MHz filter bank split into two parts of 256 channels each, in combination with VESPA. It provided a velocity resolution of 1.3 and 2.6 km s^{-1} at 1.3 and 2.7 mm, respectively. The calibration was made using the chopper wheel technique and the line intensities are reported as main beam brightness temperatures. With this setup, in some cases the same transition was observed with different velocity resolutions. The values shown in Table 3 correspond to the data with best rms.

2.3.2. Robledo de Chavela 70 m

Centimeter single-dish spectral line observations of CB 101 were obtained with NASA's 70 m antenna (DSS-63) at Robledo de Chavela, Spain, for both CCS $J_N = 2_1 \rightarrow 1_0$ and $\text{NH}_3(1,1)$ transitions. Rest frequencies, typical system temperatures, half power beam

widths, main beam efficiencies, and averaging region are given in Table 3. The rms pointing accuracy of the telescope was better than $6''$ and $11''$ for CCS and ammonia observations, respectively. The data were taken with a 1.3 cm receiver comprising a cooled high-electron-mobility transistor (HEMT) amplifier. A noise diode was used to calibrate the data. Observations were made in frequency switching mode, using a 256-channel digital Fast Fourier Transform spectrometer. The CCS observations were performed on 2002 May with a bandwidth of 1 MHz (velocity resolution $\simeq 0.05 \text{ km s}^{-1}$), while the NH_3 observations were carried out during 2003 July with a bandwidth of 10 MHz (velocity resolution $\simeq 0.5 \text{ km s}^{-1}$).

All the single-dish data reduction was carried out using the CLASS package, developed at IRAM and the Observatoire de Grenoble as part of the GAG software.

3. Results and discussion

3.1. CB 3

CB 3 is located at the near side of the Perseus arm, at a distance of $\simeq 2.5 \text{ kpc}$ (Launhardt & Henning 1997; Wang et al. 1995). This globule shows a highly luminous FIR/submillimeter dust condensation ($L_{bol} = 930 L_{\odot}$), and it seems to be associated with intermediate-mass star formation (Launhardt & Henning 1997; Launhardt et al. 1997). Several sources in different stages of evolution have been identified in CB 3: the young stellar object CB 3/YC1, which corresponds to IRAS 00259+5625 (Yun & Clemens 1994b), a near-infrared source, CB 3 YC1-I, that was proposed to be a Class II source (Yun & Clemens 1995), and a millimeter source, CB 3-mm (Launhardt & Henning 1997), cataloged by Codella & Bachiller (1999) as a probable Class 0 object, which also shows submillimeter emission (Launhardt et al. 1997). This Bok globule is associated with a bipolar molecular outflow elongated in the northeast-southwest direction (Yun & Clemens 1994b; Codella & Bachiller 1999), of which CB 3-mm was proposed to be the driving source (Codella & Bachiller 1999). The CO channel maps reveal different clumps along its main axis, which suggest episodic mass loss (Codella & Bachiller 1999). There are four H_2 emission knots, projected towards the blueshifted lobe of the outflow, and whose distribution does not follow a straight line (see Fig. 1), probably due to precession of the outflow axis (Masi et al. 2004).

Our VLA maser spectrum is shown in Fig. 1. Water maser emission in this source was first detected by Scappini et al. (1991), although the position reported with those single-dish observations is shifted $\simeq (30'', -60'')$ from our VLA position. At least five independent spectral features are evident in the VLA maser spectrum (Fig. 1), which we designated as A, B, C, D, and E on Table 2, and are centered at $\simeq -37.0, -51.4, -57.4, -67.2,$ and -78.4

km s⁻¹ respectively. Component D may in its turn be composed of two individual features, but they are blended together, given our spectral resolution. All except component A are blueshifted with respect to the cloud velocity ($V_{LSR} = -38.3$ km s⁻¹, Clemens & Barvainis 1988). The five maser features delineate a spatial structure of $\simeq 0''.1$ elongated from northeast to southwest (see Fig. 1). Assuming that the emission from a given velocity channel is dominated by a single component, its position can be determined with high accuracy. Therefore, the linear structure observed is real and it is likely to be tracing the base of a jet, since the relative positional uncertainty ($< 0''.007$, see fourth column in Table 2) of the emission for individual maser spectral features is better than the total size of the structure ($\simeq 0''.1$; see Fig. 1). The emission corresponding to the velocity closest to that of the cloud (feature A) occupies the southern part of the structure, while that of the most blueshifted one (E) is located at the north.

The maser emission is aligned in the same direction than the blueshifted molecular outflow, and it is located $\simeq 5''$ south of the position of CB3-mm reported by Launhardt & Henning (1997), between this source and the northernmost H₂ knot observed by Massi et al. (2004) (see Fig. 1). However, the mm observations were made with a beamsize of $\simeq 12''$, so it is possible that both mm and water maser emission actually come from the same location, which would be more accurately traced by the masers. The proximity of the masers to the mm source is consistent with the idea that the YSO traced by this source is exciting the water masers and probably powering the molecular outflow. Nevertheless, although this mm source is the best candidate, we cannot rule out the existence of another embedded source closer to the masers, and higher resolution observations at millimeter and submillimeter wavelengths are needed in order to clarify this point.

In Fig. 2 we have represented the position-velocity diagram of the maser emission along the major axis of the maser structure, by considering the centroids of the maser emission for each velocity channel. We note that although these centroids are not independent spectral features, spatio-kinematical information of the gas traced by water masers can be derived from the analysis of these centroids, under the assumption that each velocity channel there is a single dominant component. This diagram shows an interesting wave-like distribution, similar to that observed in AFGL 2591 (Trinidad et al. 2003). Massi et al. (2004), based on the relative spatial distribution of H₂ knots with respect to the powering source, suggested the possible presence of a precessing outflow. Our position-velocity diagram also supports this suggestion, but at smaller scales, with the wave-like distribution pattern compatible with a precessing jet traced by masers at scales of $\simeq 250$ AU. To illustrate this possibility we have represented an ideal model of a precessing jet that can qualitatively explain the same wave-like tendency observed in the position-velocity diagram. In the lower panels of Fig. 2, we show a sketch reproducing the model we propose. In order to fit the model with the

observed pattern, we approximated the precessing jet with a narrow cone on whose surface discrete ejections of material are located and we assumed that the ejected material is being decelerated (bottom left panel of Fig. 2). We also consider that the motion of the ejected material is dominated by deceleration, while the changes in velocity due to precession are negligible. Therefore, our model can reproduce a wave-like distribution (solid lines joining the dots in the bottom right panel of Fig. 2) similar to the one observed (dashed lines joining the symbols in the upper panel of Fig. 2). Under these assumptions, we estimate a deceleration of the ejected material of $\simeq 2.2 \times 10^{-8} \cos i \text{ km s}^{-2}$ ($\simeq 0.14 \cos i \text{ AU yr}^{-2}$), where i is the position angle between the direction of the jet and the plane of the sky. We caution that our aim with this model is to explain the wave-like tendency observed with the position-velocity diagram, and not to reproduce exactly the observed maser emission. Further support for the possible presence of a precessing jet at these small scales (250 AU) could be obtained with proper motions studies of masers by means of VLBI observations.

3.2. CB 54

This Bok globule hosts a multiple system of YSOs towards CB54 YC1 (IRAS 07020-1618), with the presence of two bright near-infrared (K band, $2.2 \mu\text{m}$) objects (CB54 YC1-I, YC1-II, which are probably Class I protostars), plus a bright elongated feature (hereafter CB54 YC1-SW) mainly seen in H_2 [$v = 1-0 \text{ S}(1)$, $2.121 \mu\text{m}$] (Yun & Clemens 1994a, 1995; Yun et al. 1996; see Fig. 3). In addition, Yun et al. (1996) and Moreira et al. (1997) reported a radio continuum source (CB 54 VLA1) at 3.6 and 6 cm located $\simeq 5''$ to the NE of the nominal position of the IRAS source (see Fig. 3). These sources are located near the center of a bipolar CO outflow that is oriented in the northeast-southwest direction and probably moves close to the plane of the sky (Yun & Clemens 1994b).

Our VLA observations (Fig. 3) reveal water maser emission with two distinct spectral features, at $\simeq 15.8$ and 17.8 km s^{-1} . These velocities are blueshifted with respect to the velocity of the cloud ($V_{LSR}=19.5 \text{ km s}^{-1}$; Clemens & Barvainis 1988). No maser emission was detected with the Robledo antenna at the velocities reported here (Gómez et al. 2006), which is understandable since the flux density reported here is below the sensitivity threshold of those single-dish observations. However, Gómez et al. (2006) detected a component at $\simeq 8 \text{ km s}^{-1}$, which reached a flux density of up to $\simeq 45 \text{ Jy}$, and another one of up to $\simeq 1 \text{ Jy}$ at $\simeq 14 \text{ km s}^{-1}$. Neither of these is evident in the VLA spectrum (Fig. 3), although the component at $\simeq 14 \text{ km s}^{-1}$ might be present at a very low level, and blended with the one at $\simeq 15.8 \text{ km s}^{-1}$.

The maser emission is located at the position of the elongated feature CB54 YC1-SW

(see Fig. 3). Yun (1996), on the basis that the elongated feature appears brighter in H_2 than in the K-band, proposed that it could trace shocked material, such as a knot in a near-infrared jet. However, given the association of CB 54 YC1-SW with the water masers, we suggest that this feature is another embedded YSO and that, according to the association of water masers with mass-loss phenomena, this object would be a good candidate for being the powering source of the observed molecular outflow in the region. In fact, masers are located $\simeq 18000$ - 20000 AU (at a distance of 1.5 kpc; Launhardt & Henning 1997) from both CB 54 YC1-I and CB 54 YC1-II, which make these objects less likely candidates for pumping the maser emission, since masers in low-mass star-forming regions tend to be within several hundred AU from the powering source (Chernin 1995; Claussen et al. 1998; Furuya et al. 2000, 2003). We did not detect 1.3 cm continuum emission with the VLA either at the position of CB54 YC1-SW or toward the other proposed YSOs in the region, with a 3σ upper limit of 0.4 mJy. Deeper radio continuum measurements in this region could help to confirm whether CB54 YC1-SW is indeed a YSO.

3.3. CB 65

IRAS 16277–2332 is located at the north-western edge of the Bok globule CB 65, in Ophiucus. The nature of this IRAS source is unknown, and in fact, Parker (1988) suggested that it may not be associated with the globule. Visser et al. (2002) carried out submillimeter observations towards CB 65, and detected a submillimeter core at the center of the globule at a distance of $\simeq 3'$ southeast of IRAS 16277–2332, but no emission was detected at the IRAS position. Our single dish survey with the Robledo de Chavela antenna (Gómez et al. 2006) revealed water maser emission in IRAS 16277–2332, near the CB 65 cloud velocity ($V_{LSR} = 2.3 \text{ km s}^{-1}$; Clemens & Barvainis 1988), with a peak flux density of 0.3 Jy on 2002 June 16. However, no water maser emission was detected with the VLA (≤ 40 mJy, 3σ upper limit), which is not surprising given the time variability of these masers (Reid & Moran 1981). No 1.3 cm continuum emission was detected, with a 3σ upper limit of 2.7 mJy. On the other hand, the observations performed with the IRAM 30 m antenna in the CO(1–0) and (2–1) transitions, showed no high-velocity wings in the spectra, with an rms of 0.03 K and 0.3 K respectively. This indicates the absence of any significant mass-loss activity.

Unfortunately, there is not enough information in the literature about IRAS 16277–2332 that may help us to clarify the real nature of this source. For instance, IRAS data show emission at $60 \mu\text{m}$, but only upper limits at 12, 25, and $100 \mu\text{m}$. There are no Midcourse Space Experiment (MSX) infrared data nor emission in the 2MASS K, H, or J bands, from which to obtain information about its spectral energy distribution. Deeper infrared observations

are needed to reveal the nature of this source.

3.4. CB 101

CB 101 is a Bok globule located at 200 pc (Lee & Myers 1999), and cataloged as a cold and quiescent cloud (Clemens et al. 1991) that hosts two IRAS sources, IRAS 17503–0833 and IRAS 17505–0828. Our water maser single-dish survey (Gómez et al. 2006) revealed water maser emission towards IRAS 17503–0833. This source is located $\simeq 9'$ south of the globule center.

3.4.1. Water Masers and Radio Continuum Emission

We have detected with the VLA water maser emission toward IRAS 17503–0833 at $V_{LSR} \sim 29.5 \text{ km s}^{-1}$ (see Table 2 and Fig. 4), which is redshifted with respect to the velocity of the molecular cloud ($V_{LSR} = 6.7 \text{ km s}^{-1}$; Clemens & Barvainis 1988). The flux density and velocity of the water maser emission are similar to those found with the Robledo antenna (Gómez et al. 2006). The water maser emission coincides with a point source observed in the 2MASS K-band, which is probably the near-IR counterpart of IRAS 17503–0833 (see Fig. 4). We did not detect VLA radio continuum emission at 1.3 cm, with a 3σ upper limit of 0.4 mJy.

3.4.2. Millimeter and Centimeter Single-Dish Observations

Our aim was to search for any sign of star formation activity toward IRAS 17503–0833 (e.g., presence of molecular outflows, high density molecular gas, and/or shocked material). We mapped the CO($J = 1 \rightarrow 0$) and ($J = 2 \rightarrow 1$) transitions over an area of $40'' \times 40''$ in order to detect a possible molecular outflow in the region. No high-velocity emission was detected in the spectra of any of these transitions, with a rms of 0.012 K per channel (channel width $\simeq 0.8 \text{ km s}^{-1}$) and 0.026 K per channel (channel width $\simeq 0.4 \text{ km s}^{-1}$), respectively. Moreover, as for the general distribution of the molecular gas, Fig. 5 shows the map of $^{13}\text{CO}(J = 1 \rightarrow 0)$ integrated intensity in a region of $2' \times 2'$. It reveals more intense emission towards the northwest of the IRAS source, which probably originates from the molecular gas contained in the Bok globule, but there is no obvious local maximum of molecular gas towards the source. In Table 3 we summarized the parameters of the single-dish spectra of different molecular transitions towards IRAS 17503–0833.

The $^{13}\text{CO}(J = 2 \rightarrow 1)$ emission is weak, and barely detectable in the region (Fig. 5). We did not detect emission of high-density molecular gas tracers such as the $\text{CCS}(2_1-1_0)$, $\text{NH}_3(1,1)$, $\text{CS}(J = 2 \rightarrow 1)$ and $\text{CS}(J = 5 \rightarrow 4)$ lines. No emission of the $\text{SiO}(J = 2 \rightarrow 1)$ transition was detected either. This transition is usually associated with shocked regions around young stellar objects (Harju et al. 1998; Gibb et al. 2004).

We derived the physical conditions from the CO and ^{13}CO spectra obtained towards the IRAS source, under the following three assumptions (Estalella & Anglada 1996): (1) local thermodynamic equilibrium, (2) the CO emission is optically thick, and (3) ^{13}CO emission is optically thin. The $\text{CO}(J = 1 \rightarrow 0)$ emission towards the IRAS position was used to obtain the excitation temperature (T_{ex}) from:

$$T_{\text{ex}} = 5.53 \left[\ln \left(1 + \frac{5.53}{T_{\text{CO}} + 0.82} \right) \right]^{-1} K,$$

where T_{CO} is the main beam brightness temperature of the $\text{CO}(J = 1 \rightarrow 0)$ emission, in K.

For the $^{13}\text{CO}(J = 1 \rightarrow 0)$ we derived its optical depth ($\tau_{^{13}\text{CO}}$) and its column density $N(^{13}\text{CO})$ as:

$$\tau_{^{13}\text{CO}} = -\ln \left[1 - T_{^{13}\text{CO}} \left(\frac{5.29}{\exp(5.29/T_{\text{ex}}) - 1} - 0.87 \right)^{-1} \right],$$

$$N(^{13}\text{CO}) = 2.42 \times 10^{14} \frac{T_{\text{ex}} \Delta v \tau_{^{13}\text{CO}}}{1 - \exp(-5.29/T_{\text{ex}})} \text{ cm}^{-2},$$

where $T_{^{13}\text{CO}}$ is the main beam brightness temperature of the $^{13}\text{CO}(J = 1 \rightarrow 0)$ emission in K, and Δv is the line width at half maximum, in km s^{-1} .

The physical parameters (derived from the spectra shown in Fig. 5 and their corresponding values in Table 3), are $T_{\text{ex}} = 9.6 \pm 0.3$ K, $\tau_{^{13}\text{CO}} = 0.27 \pm 0.07$, and $N(^{13}\text{CO}) = (6.6 \pm 2.6) \times 10^{14} \text{ cm}^{-2}$ at the position of the IRAS source. The value of $N(\text{H}_2)$ is $(3.3 \pm 1.2) \times 10^{20} \text{ cm}^{-2}$, derived from the relative abundance of ^{13}CO with respect to H_2 , proposed by Dickman (1978), $[\text{H}_2/^{13}\text{CO}] = 5 \times 10^5$. Kim & Hong (2002) reported a value of $N(^{13}\text{CO}) = 3.7 \times 10^{15} \text{ cm}^{-2}$ towards the central peak position of CB 101 (located $\simeq 9'$ north). This value at the center of the globule is $\simeq 6$ times higher than the value derived by us at the position of IRAS 17503–0833, which is consistent with a decrease of the gas density towards the edges of the cloud.

3.4.3. *The Nature of IRAS 17503–0833*

The absence of any signpost of star formation activity associated with the water maser emission, suggests that the water maser in CB 101 may not be associated with a young object but with an evolved star, since water maser emission is also known to be associated with circumstellar envelopes of late-type stars (Bowers & Hagen 1984; Engels et al. 1986, 1988; Habing 1996). Moreover, the difference between the centroid velocity of the detected water maser and the cloud velocity is $\simeq 23 \text{ km s}^{-1}$, whereas this difference is usually $\leq 15 \text{ km s}^{-1}$ in the case of YSOs (Wilking et al. 1994; Anglada et al. 1996; Brand et al. 2003). To further investigate the true nature of IRAS 17503–0833, we searched for additional data in the literature.

The IRAS flux density at $12 \mu\text{m}$ is well determined, but the values for 25, 60, and $100 \mu\text{m}$ are only upper limits. The near-infrared flux densities were retrieved from the 2MASS catalog, and dereddened with a value for $E(B-V) = 0.21$, taken from Whitelock et al. (1986) for stars with galactic latitude $b = 8 \text{ deg}$. The corrected J, H, and K magnitudes are: 8.643, 7.690, and 7.100, respectively. The near- and far-infrared data flux densities are shown in Table 4, where we do not include the IRAS flux density at $100 \mu\text{m}$ due to the low quality of those data.

In Fig. 5 we have plotted the spectral energy distribution (SED) of IRAS 17503–0833, including the upper limits for the IRAS flux densities. Evolved objects may show one or two maxima in their SED. After the AGB the SEDs usually show two maxima, one belonging to the central star and the other to the circumstellar envelope (Kwok 1993). In the case of IRAS 17503–0833, if it is an evolved object there seem to be only one maximum in the near infrared; the second maximum should have shown up in the far infrared. The presence of only one maximum suggests that no disk or circumstellar envelope is detached from the central star. This would restrict the evolutionary stage of the star to the phase between Red Giant and the Asymptotic Giant Branch (AGB). The SED is then compatible with a black body distribution at a temperature of $\simeq 2200 \text{ K}$, although more data points at different wavelengths would be necessary to better constrain this temperature. In Fig. 5, we have plotted the dereddened IR colours of the object in an IR color-color diagram, to further check its evolutionary stage. IRAS 17503–0833 is located to the right and above the Main Sequence and the Red Giant Branch, which is typical of Mira stars (see Whitelock et al. 1994, 1995). The temperatures of these stars fall in the range between 2000 K and 3500 K (van Belle et al. 2002), which is compatible with the temperature of $\sim 2200 \text{ K}$ estimated by us. Moreover, water maser emission is very frequent in Mira-type stars (Bowers & Hagen 1984). Therefore, we suggest that the CO emission found belongs to the cloud CB 101, and IRAS 17503–0833 is a field star, not associated with the cloud. This is consistent with the

location of this source at the edge of the Bok globule, at a distance of $\simeq 9'$ from its center. In any case, additional observations at other frequencies, in order to be able to accurately determine the effective temperature of the star from the SED, together with a light curve to perform variability studies of this source are needed to confirm its identification as a Mira star.

3.5. CB 205

CB 205, at a distance of 2 kpc (Launhardt & Henning 1997), is a very active star formation region containing several YSOs (Herbst & Turner 1976; Neckel et al. 1985; Neckel & Staude 1990; Huard et al. 2000; Massi et al. 2004), and a weakly collimated bipolar molecular outflow with a significant overlapping of the redshifted and blueshifted emission lobes (Xie & Goldsmith 1990).

CB 205 is one of the few Bok globules in the CB catalog where water maser emission was known (Neckel et al. 1985) before the survey of Gómez et al. (2006). The maser, located near IRAS 19433+2743, showed a peak flux density of $\simeq 4.8$ Jy on May–October 1983. This emission was detected again by Brand et al. (1994) on 1992 January 18, with a peak flux density of 0.7 Jy and located $\simeq 40''$ west of our phase center, although inside the $2'$ VLA primary beam at 22 GHz. However, Gómez et al. (2006) did not detect the maser, with a 3σ upper limit of 0.75 Jy on 2003 July 11 and of 0.15 Jy on 2004 July 22 and 2005 June 16. Our VLA observations also failed to detect any water maser emission on 2004 February 3, at a level of $\gtrsim 7$ mJy (3σ). In our VLA observations, we did not detect any radio continuum emission at 1.3 cm, with a 3σ upper limit of 0.5 mJy.

3.6. CB 232

This Bok globule contains a CO bipolar molecular outflow centered near CB 232 YC1 (IRAS 21352+4307), whose lobes are slightly overlapped and exhibit a poor degree of collimation (Yun & Clemens 1994b). Near-infrared maps reveal a single source, the possible counterpart of IRAS 21352+4307 (Yun & Clemens 1994a), which was designated as CB 232 YC1-I and classified as a Class I object by Yun & Clemens (1995). Huard et al. (1999) detected two submillimeter sources, SMM1 (the westernmost one) and SMM2 (the easternmost one), located $\simeq 10''$ west and $\simeq 5''$ south-east from CB 232 YC1-I respectively, with a positional error of $\simeq 4''$. SMM1 was classified as a Class 0 source while SMM2 was proposed to be either the submillimeter counterpart of CB 232 YC1-I, or another Class 0 source without

infrared counterpart (Huard et al. 1999).

Our VLA observations show water maser emission with velocity $V_{LSR} \sim 10.1 \text{ km s}^{-1}$ (see Table 2 and Fig. 6), close to the cloud velocity ($V_{LSR}=12.6 \text{ km s}^{-1}$; Clemens & Barvainis 1988), and coinciding, within the positional uncertainty, with the position of the near-infrared source CB 232 YC1-I (see Fig. 6). This positional agreement favors CB 232 YC1-I as the most likely candidate to power the maser emission and the molecular outflow observed in the region (according to the typical association of water masers to mass-loss phenomena).

The velocity of the maser is consistent with that found in the single-dish detection by Gómez et al. (2006), although the flux density was a factor of ~ 50 larger at the epoch of our interferometric observations. We did not detect radio continuum emission at 1.3 cm, with a 3σ upper limit of 0.5 mJy.

4. Conclusions

In this work we have presented interferometric observations using the VLA, of several sources of water maser emission detected as part of a single-dish survey performed with the Robledo-70m antenna towards Bok globules. The general conclusions we have obtained are the following:

- We have detected water maser emission with the VLA in CB 3, CB 54, CB 101 and CB 232. No water maser emission was detected towards CB 65 or CB 205.
- These water masers are associated with star forming regions showing bipolar molecular outflows, except for CB 101 (IRAS 17503–0833), which we propose is an evolved object, possibly a Mira star, and CB 65 (IRAS 16277–2332), whose nature is unknown.
- All of the Bok globules associated with star formation present multiple stellar systems in different evolutionary stages. Accurate positions of water masers has helped us to get information about the powering sources in the case of CB 3, CB 54, and CB 232. We propose the millimeter source CB 3-mm and the near-IR source CB 232 YC1-I as the best candidates for pumping the maser emission in CB 3 and CB 232 respectively. In the case of CB 54, we propose a new young object (CB 54 YC1-SW), seen as an elongated feature in near-infrared images, as the powering source of the maser emission.
- The maser emission in CB 3 is distributed along the direction of the molecular outflow, and seems to be tracing the inner part of a collimated jet. The position-velocity distribution of the maser emission shows a wave-like structure, which is consistent with a precessing jet.

The authors thank the valuable comments of our anonymous referee, which have greatly improved this work. We are also thankful to Fabrizio Massi for providing the near-infrared data in CB 3 and David Barrado y Navascués for his help with the data reduction of this image. GA, JFG, and JMT acknowledge support from the Ministry of Science and Technology (MCYT) grant (European Fund of Regional Development, FEDER) AYA2005-08523-C03 (Spain), and OS acknowledges support from the grant AYA 2003-09499. GA and JFG acknowledge support from Junta de Andalucía (TIC-126). IdG acknowledges the support from a Calvo Rodés Fellowship from the Instituto Nacional de Técnica Aeroespacial (INTA). The work by TBHK was done at the Jet Propulsion Laboratory, California Institute of Technology, under contract to the National Aeronautics and Space Administration (NASA). JMT acknowledges the high hospitality of the UK Astronomy Technology Centre, Royal Observatory Edinburgh, during his sabbatical stay. This paper is partly based on observations taken during “host-country” time allocated at Robledo de Chavela; this time is managed by the Laboratorio de Astrofísica Espacial y Física Fundamental (LAEFF) of INTA, under agreement with National Aeronautics and Space Administration/Ingeniería y Servicios Aeroespaciales (NASA/INSA). It also makes use of data products from the Two Micron All Sky Survey (2MASS), which is a joint project of the University of Massachusetts and the Infrared Processing and Analysis Center/California Institute of Technology, funded by NASA and the National Science Foundation.

REFERENCES

- André, P., Ward-Thompson, D., & Barsony, M. 1993, *ApJ*, 406, 122
- André, P. & Montmerle, T. 1994, *ApJ*, 420, 837
- Anglada, G. 1995, *Revista Mexicana de Astronomía y Astrofísica Conference Series*, 1, 67
- Anglada, G., Estalella, R., Pastor, J., Rodríguez, L. F., & Haschick, A. D. 1996, *ApJ*, 463, 205
- Brand, J., Cesaroni, R., Comoretto, G., Felli, M., Palagi, F., Palla, F., & Valdetaro, R. 2003, *A&A*, 407, 573
- Bok, B. J., & Reilly, E. F. 1947, *ApJ*, 105, 255
- Bourke, T. L., Hyland, A. R., Robinson, G., James, S. D., & Wright, C. M. 1995, *MNRAS*, 276, 1067
- Bowers, P. F., & Hagen, W. 1984, *ApJ*, 285, 637
- Brand, J., Cesaroni, R., Caselli, P., Catarzi, M., Codella, C., Comoretto, G., Curioni, G. P., Curioni, P., di Franco, S., Felli, M., Giovanardi, C., Olmi, L., Palagi, F., Palla, F., Panella, D., Pareschi, G., Rossi, E., Speroni, N., & Tofani, G. 1994, *A&AS*, 103, 541
- Brand, J., Cesaroni, R., Comoretto, G., Felli, M., Palagi, F., Palla, F., & Valdetaro, R. 2003, *A&A*, 407, 573
- Chernin, L. M. 1995, *ApJ*, 440, L97
- Claussen, M. J., Marvel, K. B., Wootten, A., & Wilking, B. A. 1998, *ApJ*, 507, L79
- Clemens, D. P. & Barvainis, R. 1988, *ApJS*, 68, 257 (CB)
- Clemens, D. P., Yun, J. L., & Heyer, M. H. 1991, *ApJS*, 75, 877
- Codella, C. & Bachiller, R. 1999, *A&A*, 350, 659
- Codella, C., Palumbo, G. G. C., Pareschi, G., Scappini, F., Caselli, P., & Attolini, M. R. 1995, *MNRAS*, 276, 57
- De Buizer, J. M., Radomski, J. T., Telesco, C. M., & Piña, R. K. 2005, *ApJS*, 156, 179
- Dickman, R. L. 1978, *ApJS*, 37, 407

- Elitzur, M., Hollenbach, D. J., & McKee, C. F. 1989, *ApJ*, 346, 983
- Elitzur, M., Hollenbach, D. J., & McKee, C. F. 1992, *ApJ*, 394, 221
- Engels, D., Schmid-Burgk, J., & Walmsley, C. M. 1986, *A&A*, 167, 129
- Engels, D., Schmid-Burgk, J., & Walmsley, C. M. 1988, *A&A*, 191, 283
- Estalella, R., & Anglada, G. 1996, *Introducción a la Física del Medio Interestelar. Textos docents*, 50 (Edicions de la Universitat de Barcelona; Barcelona)
- Felli, M., Palagi, F., & Tofani, G. 1992, *A&A*, 255, 293
- Fiebig, D., Duschl, W. J., Menten, K. M., & Tscharnuter, W. M. 1996, *A&A*, 310, 199
- Furuya, R. S., Kitamura, Y., Wootten, H. A., Claussen, M. J., Saito, M., Marvel, K. B., & Kawabe, R. 2000, *ApJ*, 542, L135
- Furuya, R. S., Kitamura, Y., Wootten, H. A., Claussen, M. J., & Kawabe, R. 2001, *ApJ*, 559, L143
- Furuya, R. S., Kitamura, Y., Wootten, A., Claussen, M. J., & Kawabe, R. 2003, *ApJS*, 144, 71
- Gibb, A. G., Richer, J. S., Chandler, C. J., & Davis, C. J. 2004, *ApJ*, 603, 198
- Goddi, C., Moscadelli, L., Alef, W., Tarchi, A., Brand, J., & Pani, M. 2005, *A&A*, 432, 161
- Goldreich, P. & Kwan, J. 1974, *ApJ*, 191, 93
- Gómez, J. F., de Gregorio-Monsalvo, I., Suárez, O., & Kuiper, T. B. H. 2006, *AJ*, 132, 1322
- Habing, H. J. 1996, *A&A Rev.*, 7, 97
- Harju, J., Lehtinen, K., Booth, R. S., & Zinchenko, I. 1998, *A&AS*, 132, 211
- Herbst, W. & Turner, D. G. 1976, *PASP*, 88, 308
- Hirano, N., Liu, S.-Y., Shang, H., Ho, P. T. P., Huang, H.-C., Kuan, Y.-J., McCaughrean, M. J., & Zhang, Q. 2006, *ApJ*, 636, L141
- Huard, T. L., Sandell, G., & Weintraub, D. A. 1999, *ApJ*, 526, 833
- Huard, T. L., Weintraub, D. A., & Sandell, G. 2000, *A&A*, 362, 635
- Kane, B. D., & Clemens, D. P. 1997, *AJ*, 113, 1799

- Kim, H. G., & Hong, S. S. 2002, *ApJ*, 567, 376
- Kwok, S. 1993, *ARA&A*, 31, 63
- Launhardt, R. & Henning, T. 1997, *A&A*, 326, 329
- Launhardt, R., Ward-Thompson, D., & Henning, T. 1997, *MNRAS*, 288, L45
- Lee, C. W., & Myers, P. C. 1999, *ApJS*, 123, 233
- Marvel, K. B. 2005, *AJ*, 130, 2732
- Massi, F., Codella, C., & Brand, J. 2004, *A&A*, 419, 241
- Menten, K. M., & van der Tak, F. F. S. 2004, *A&A*, 414, 289
- Moreira, M. C., Yun, J. L., Torrelles, J. M., Afonso, J. M., & Santos, C. A. 1999, *AJ*, 118, 1315
- Moreira, M. C., Yun, J. L., Vázquez, R., & Torrelles, J. M. 1997, *AJ*, 113, 1371
- Moscadelli, L., Cesaroni, R., & Rioja, M. J. 2000, *A&A*, 360, 663
- Neckel, T., Chini, R., Guesten, R., & Wink, J. E. 1985, *A&A*, 153, 253
- Neckel, T. & Staude, H. J. 1990, *A&A*, 231, 165
- Palla, F., & Prusti, T. 1993, *A&A*, 272, 249
- Parker, N. D. 1988, *MNRAS*, 235, 139
- Patel, N. A., Greenhill, L. J., Herrnstein, J., Zhang, Q., Moran, J. M., Ho, P. T. P., & Goldsmith, P. F. 2000, *ApJ*, 538, 268
- Persi, P., Palagi, F., & Felli, M. 1994, *A&A*, 291, 577P
- Reid, M. J. & Moran, J. M. 1981, *ARA&A*, 19, 231
- Rodríguez, L. F., Moran, J. M., Gottlieb, E. W., & Ho, P. T. P. 1980, *ApJ*, 235, 845
- Scappini, F., Caselli, P., & Palumbo, G. G. C. 1991, *MNRAS*, 249, 763
- Schwartz, P. R. & Buhl, D. 1975, *ApJ*, 201, L27
- Seth, A. C., Greenhill, L. J., & Holder, B. P. 2002, *ApJ*, 581, 325
- Shu, F. H., Adams, F. C., & Lizano, S. 1987, *ARA&A*, 25, 23

- Torrelles, J. M., Gómez, J. F., Rodríguez, L. F., Curiel, S., Anglada, G., & Ho, P. T. P. 1998, *ApJ*, 505, 756
- Torrelles, J. M., Gomez, J. F., Rodríguez, L. F., Curiel, S., Ho, P. T. P., & Garay, G. 1996, *ApJ*, 457, L107
- Torrelles, J. M., Gómez, J. F., Rodríguez, L. F., Ho, P. T. P., Curiel, S., & Vázquez, R. 1997, *ApJ*, 489, 744
- Torrelles, J. M., Patel, N. A., Anglada, G., Gómez, J. F., Ho, P. T. P., Lara, L., Alberdi, A., Cantó, J., Curiel, S., Garay, G., & Rodríguez, L. F. 2003, *ApJ*, 598, L115
- Trinidad, M. A., Curiel, S., Cantó, J., D'Alessio, P., Rodríguez, L. F., Torrelles, J. M., Gómez, J.F., Patel, N., Ho, P. T. P. 2003, *ApJ*, 589, 386
- van Belle, G. T., Thompson, R. R., & Creech-Eakman, M. J. 2002, *AJ*, 124, 1706
- Visser, A. E., Richer, J. S., & Chandler, C. J. 2002, *AJ*, 124, 2756
- Vlemmings, W. H. T., Diamond, P., van Langevelde, H. J., Torrelles, J, M. 2006, *A&A*, 448, 597
- Wang, Y., Evans, N. J., Zhou, S., & Clemens, D. P. 1995, *ApJ*, 454, 217
- Whitelock, P., Feast, M., & Catchpole, R. 1986, *MNRAS*, 222, 1
- Whitelock, P., Menzies, J., Feast, M., Catchpole, R., Marang, F., & Carter, B. 1995, *MNRAS*, 276, 219
- Whitelock, P., Menzies, J., Feast, M., Marang, F., Carter, B., Roberts, G., Catchpole, R., & Chapman, J. 1994, *MNRAS*, 267, 711
- Wiling, B. A., Claussen, M. J., Benson, P. J., Myers, P. C., Terebey, S., & Wootten, A. 1994, *ApJ*, 431, L119
- Wouterloot, J. G. A., Brand, J., & Fiegle, K. 1993, *A&AS*, 98, 589
- Xiang, D. & Turner, B. E. 1995, *ApJS*, 99, 121
- Xie, T. & Goldsmith, P. F. 1990, *ApJ*, 359, 378
- Yun, J. L., & Clemens, D. P. 1990, *ApJ*, 365, L73
- Yun, J. L. & Clemens, D. P. 1994a, *AJ*, 108, 612

Yun, J. L. & Clemens, D. P. 1994b, ApJS, 92, 145

Yun, J. L. & Clemens, D. P. 1995, AJ, 109, 742

Yun, J. L., Moreira, M. C., Torrelles, J. M., Afonso, J. M., & Santos, N. C. 1996, AJ, 111, 841

Yun, J. L. 1996, AJ, 111, 930

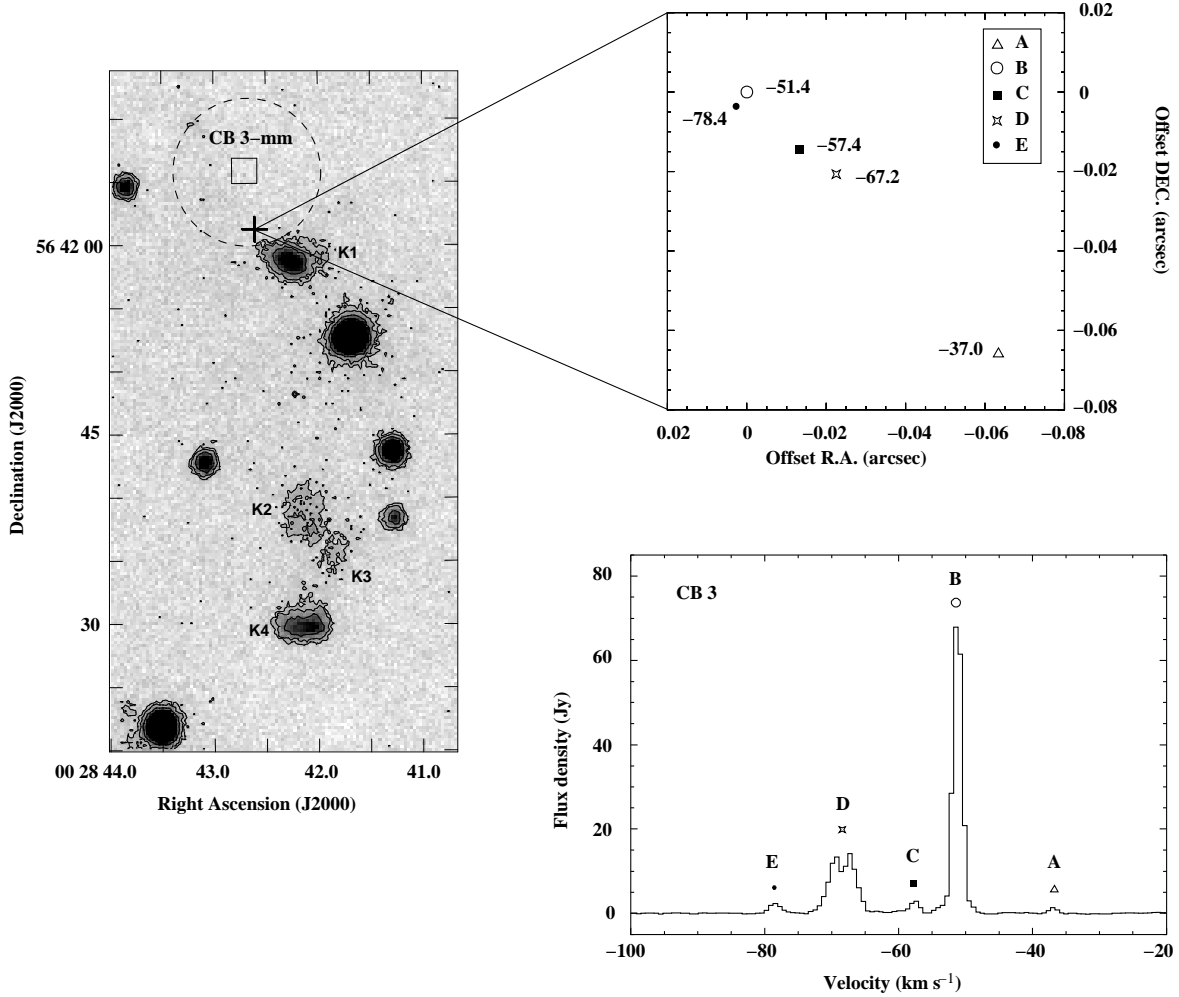


Fig. 1.— (Left) H₂ image (grey scale; Massi et al. 2004; astrometric accuracy of the image $\simeq 1''$) of CB 3. K1, K2, K3, and K4 represent the H₂ knots detected by Massi et al. 2004. The square marks the position of CB 3-mm (Launhardt & Henning 1997) and the dashed circle represents the beamsize of their millimeter observations ($\simeq 12''$). The cross marks the centroid position of the water maser emission detected with the VLA. (Lower right) Water maser spectrum of CB 3 obtained with the VLA. Different symbols correspond to the spectral features A, B, C, D, and E, indicated in Table 2. (Upper right) Spatial distribution of the independent maser spectral features showing a linear structure. The LSR velocity (in km s⁻¹) of each feature is shown. The (0,0) position in this map is the position of the reference feature used for self-calibration (Table 2).

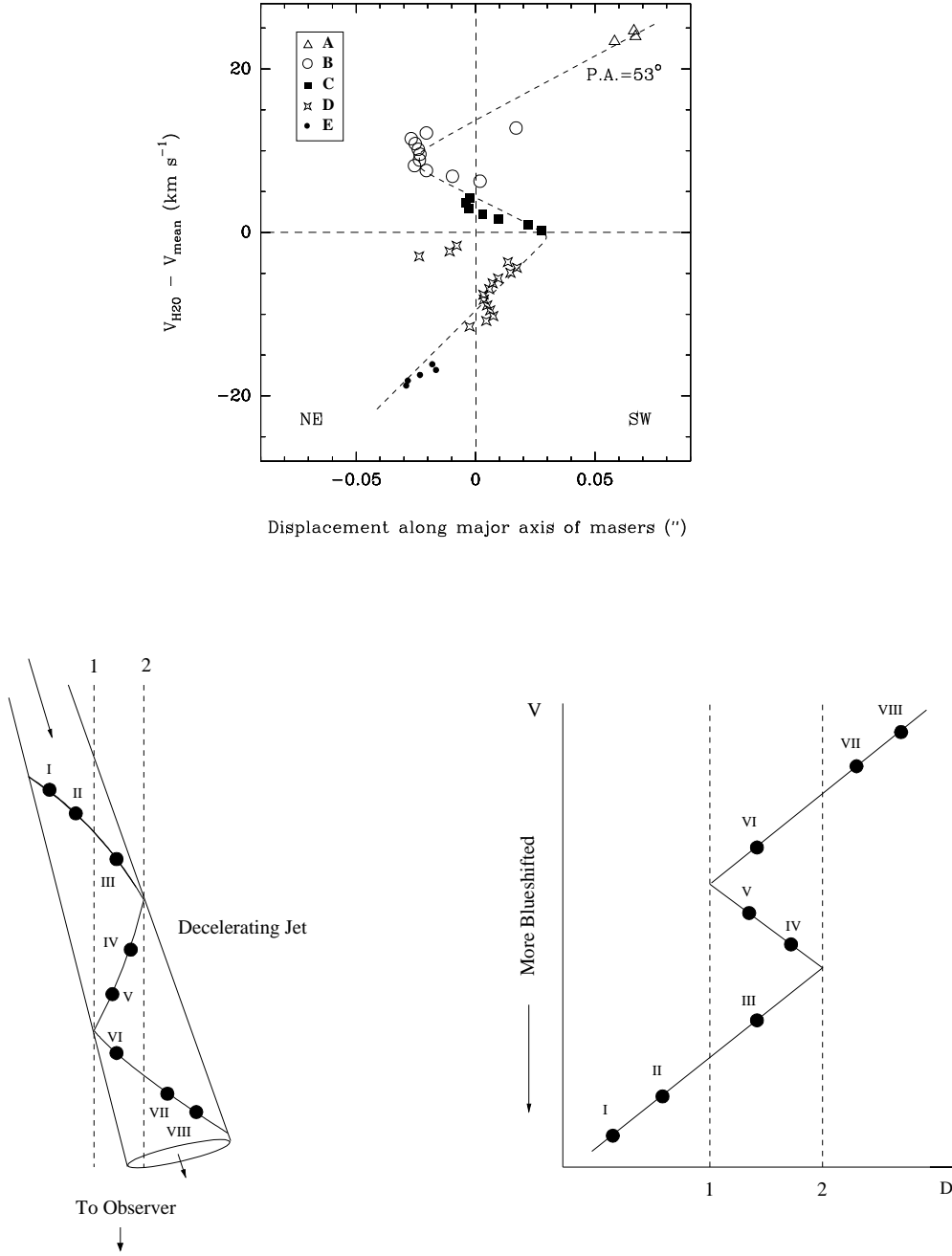


Fig. 2.— (Top) Position-velocity distribution of the centroids of the water maser emission at different velocity channels in CB 3, along the major axis of the elongated maser distribution shown in Fig. 1. The horizontal axis represents the relative position of the emission along the major axis (P.A. = 53°) of the distribution with respect to their geometrical center. The vertical axis represents the velocity of each channel after subtracting the mean velocity of the spectrum (-61.0 km s^{-1}). The mean velocity is the sum of the velocity of the channels where maser emission is observed, divided by the total number of those channels. The geometric center (Offset R.A., Offset Dec.)=(0,0) is defined as the sum of the positional offsets (in R.A. or in Dec.) of the centroid of a single dominant component of water masers at each channel where emission is observed, divided by the total number of those channels. Different symbols correspond to the same spectral features indicated in Fig. 1. The dashed line represent the general trend shown by the maser spots in this diagram. We note that points further away from the dashed line are those with the largest positional uncertainty. (Bottom left) Model of a decelerating and precessing jet. Filled circles represent hypothetical parcels of gas moving in the direction of the arrow. Dashed lines represent two lines of sight through the jet. The observer would be looking from the bottom of the page. (Bottom right) Position-velocity distribution for the proposed model. Filled circles and dashed lines correspond to their equivalent in the left panel masers along the projected main axis of the jet. The filled circles do not try to reproduce the real water maser emission at different velocity channels, but the general tendency described by them (dotted line in top panel).

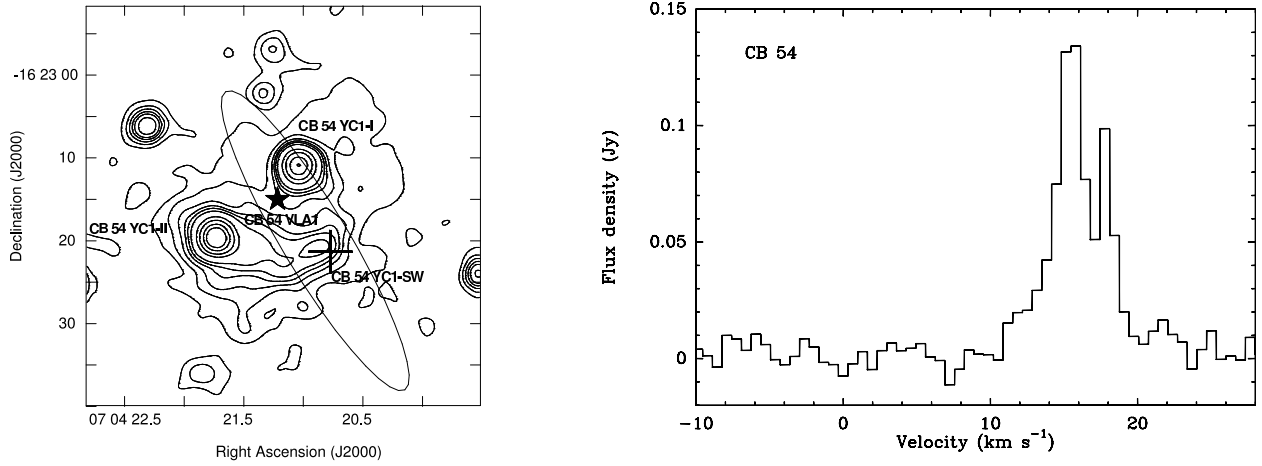


Fig. 3.— (Left panel) Contour map of the 2MASS K-band emission (positional error $\simeq 0''.2$) surrounding IRAS 07020–1618 in CB 54. The ellipse is the position error of the IRAS source. The cross indicates the centroid position of the water masers observed with the VLA. The star is the position of CB 54 VLA1, the radio continuum source at 3.6 cm reported by Yun et al. (1996; positional error $\simeq 2''$). (Right panel) Water maser spectrum of CB 54 obtained with the VLA.

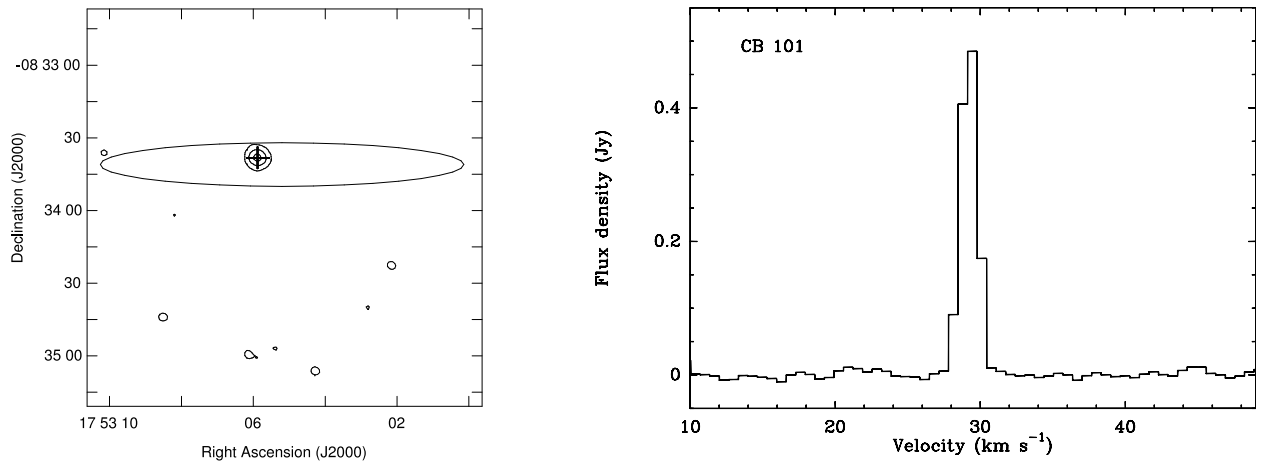


Fig. 4.— (Left panel) Contour map of the K-band 2MASS emission (positional error $\simeq 0''.14$) around IRAS 17503–0833 in CB 101. The cross represents the centroid position of the water maser emission. The ellipse represents the position error of IRAS 17503–0833. (Right panel) Water maser spectrum toward IRAS 17503–0833 in CB101, obtained with the VLA.

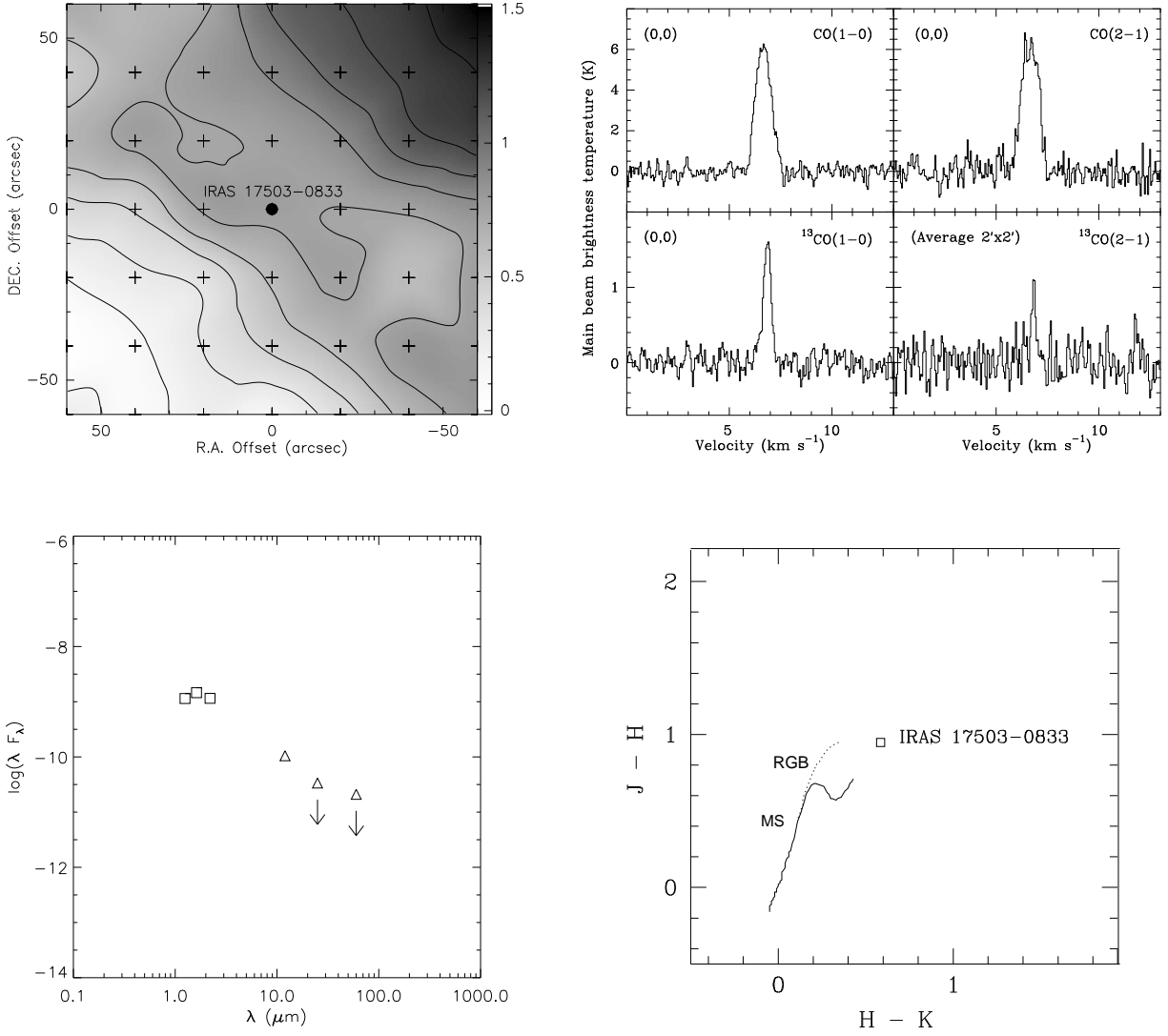


Fig. 5.— (Upper left) Map of the $^{13}\text{CO}(J = 1 \rightarrow 0)$ integrated emission in CB 101. The reference position (filled circle) is that of IRAS 17503-0833. Contour levels are represented from 0.15 to 1.5 K km s^{-1} in steps of 0.15 K km s^{-1} . Crosses mark the observed positions. (Upper right) Spectra of $\text{CO}(J = 1 \rightarrow 0)$, $\text{CO}(J = 2 \rightarrow 1)$, $^{13}\text{CO}(J = 1 \rightarrow 0)$, and $^{13}\text{CO}(J = 2 \rightarrow 1)$ at the position of IRAS 17503-0833 in CB 101. The $^{13}\text{CO}(J = 2 \rightarrow 1)$ spectrum (lower right) is the average over an area of $\simeq 2' \times 2'$ centered at the position of the IRAS source. (Lower left) Infrared spectral energy distribution of IRAS 17503-0833 in CB 101. The squares represent the 2MASS measurements in the H, J, and K band and the triangles represent the IRAS measurements at 12, 25, and 60 μm (see Table 4). (Lower right) Location of IRAS 17503-0833 in an $(H-K)$ - $(J-H)$ color diagram. The square represents the dereddened infrared color of IRAS 17503-0833. The solid line represents the main sequence, and the dotted line represents the Red Giant Branch.

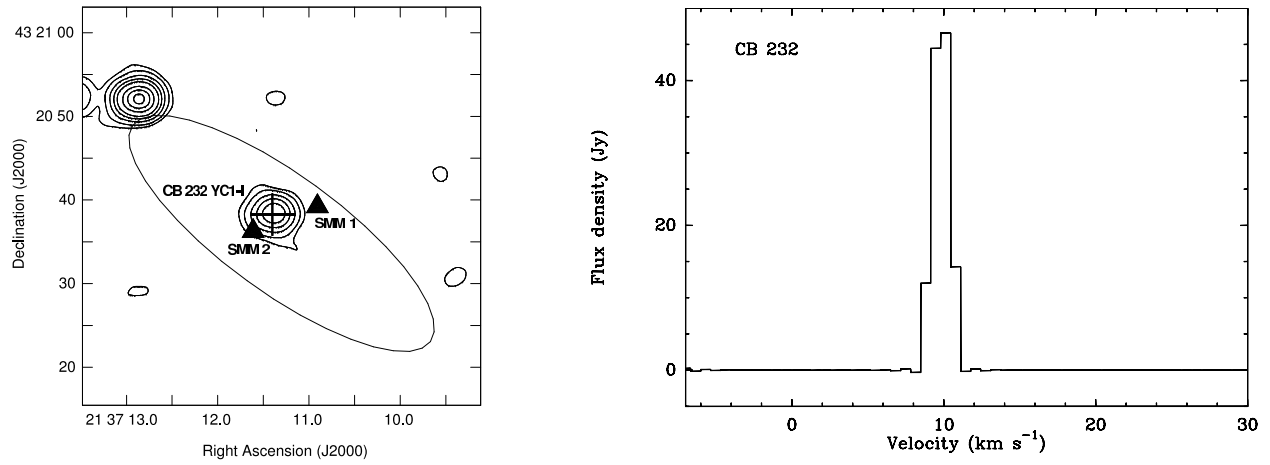


Fig. 6.— (Left panel) Contour map of the near-infrared emission in K-band (astrometric accuracy of the image $\simeq 0''.12$) around IRAS 21352+4307. The ellipse represents the error in the position of the IRAS source. The cross represents the position of the water maser emission, and the triangles mark the position of the submillimeter sources reported by Huard et al. (1999; positional error $\simeq 4''$). (Right panel) Water maser spectrum of CB 232, obtained with the VLA.

Table 1. Setup of VLA observations

Source	R.A. ^a (J2000)	Dec. ^a (J2000)	V_0^b (km s^{-1})	Beam Size ($''$)	Beam P.A. (deg)	Phase calibrator	S_{cal}^c (Jy)	Date ^d
CB 3 ^e	00 28 43.5075	+56 41 56.868	−60.0	0.55×0.25	81	J0136+478	5.8±1.2	95/10/28
CB 54	07 04 21.2170	−16 23 15.000	7.9	0.93×0.44	73	J0609−157	4.55±0.17	04/02/02
CB 65	16 30 43.7109	−23 39 07.736	2.3	0.28×0.18	86	J1626−298	2.00±0.03	05/02/12
CB 101	17 53 05.2300	−08 33 41.170	28.8	0.99×0.39	68	J1743−038	7.04±0.05	04/02/03
CB 205	19 45 23.8630	27 50 57.840	13.2	0.86×0.79	48	J2015+371	3.06±0.05	04/02/03
CB 232	21 37 11.3100	43 20 36.260	12.1	1.08×0.67	53	J2202+422	2.50±0.04	04/02/03

^aCoordinates of the phase center. Units of right ascension are hours, minutes, and seconds. Units of declination are degrees, arcminutes, and arcseconds.

^bLocal standard of rest velocity of the center of the bandwidth.

^cBootstrapped flux densities of phase calibrators at 22 GHz. Uncertainties are 2σ .

^dObservation date, YY/MM/DD

^eArchive data

Table 2. Water maser features detected with the VLA.

Source	Offset R.A. ^a ($''$)	Offset Dec. ^a ($''$)	Position ^b uncertainty ($''$)	Flux density ^c (Jy)	V_{LSR}^d (km s^{-1})
CB 3 (A)	−0.063	−0.065	0.007	1.29±0.03	−37.0
(B)	0	0	... ^e	68.19±0.04	−51.4
(C)	−0.013	−0.014	0.003	2.77±0.03	−57.4
(D)	−0.0226	−0.0207	0.0006	19.78±0.04	−67.2
(E)	0.003	−0.003	0.003	2.86±0.03	−78.4
CB 54	−6.49	−6.30	0.03	0.087±0.005	17.8
	−6.467	−6.293	0.018	0.129±0.005	15.8
CB 101	0	0	... ^e	0.499±0.003	29.5
CB 232	0	0	... ^e	46.568±0.006	10.1

^aPosition offsets of the peak of each distinct water maser feature with respect to the reference feature used for self-calibration, which are (R.A., Dec.)_{J2000.0} = (00 28 42.612, 56 42 01.17) for CB 3, (17 53 05.882, −08 33 38.17) for CB 101 and (21 37 11.402, 43 20 38.26) for CB 232, or with respect to the phase center (07 04 21.217, −16 23 15.00) for CB 54. Units of right ascension are hours, minutes, and seconds. Units of declination are degrees, arcminutes, and arcseconds.

^bUncertainty in the relative positions with respect to the reference positions. The absolute position uncertainty of the reference position is $\simeq 0''.19$ for CB 3, $\simeq 0''.05$ for CB 101, and $\simeq 0''.12$ for CB 232 and CB 54. Uncertainties are 2σ .

^cQuoted uncertainties are two times the rms noise in the maps.

^dLSR velocity of the spectral features. Velocity resolution $\sim 1.3 \text{ km s}^{-1}$.

^eReference feature.

Table 3. Single-dish observations towards CB 101 and CB 65

Molecule	Transition	ν_0 (MHz)	Telescope	δv^a (km s ⁻¹)	T_{sys}^b (K)	HPBW ^c ($''$)	η_{MB}^d	T_{MB}^e (K)	Averaging ^f area ($' \times '$)	Δv^g (km s ⁻¹)	$\int T_{\text{MB}} dv^h$ (K km s ⁻¹)
CB 65											
CO	$J = 1 \rightarrow 0$	115271.2018	IRAM-30m	2.60	400	21	0.73	<0.03	(0,0)
	$J = 2 \rightarrow 1$	230538.0000	IRAM-30m	1.30	600	11	0.52	<0.3	(0,0)
CB 101											
¹³ CO	$J = 1 \rightarrow 0$	110201.3541	IRAM-30m	0.05	270	22	0.74	1.51±0.23	(0,0)	0.44±0.04	0.61±0.16
	$J = 2 \rightarrow 1$	220398.6765	IRAM-30m	0.05	2700	11	0.54	1.1±0.5	2×2	0.24±0.09	0.27±0.21
C ¹⁸ O	$J = 1 \rightarrow 0$	109782.1734	IRAM-30m	0.05	290	22	0.74	<0.10	2×2
	$J = 2 \rightarrow 1$	219560.3568	IRAM-30m	0.05	1300	11	0.54	<0.4	2×2
CO	$J = 1 \rightarrow 0$	115271.2018	IRAM-30m	0.05	400	21	0.73	6.3±0.6	(0,0)	0.86±0.03	5.7±0.7
	$J = 2 \rightarrow 1$	230538.0000	IRAM-30m	0.05	600	11	0.52	6.6±1.0	(0,0)	0.95±0.05	6.4±1.5
SiO	$J = 2 \rightarrow 1$	86846.9600	IRAM-30m	0.07	700	28	0.77	<0.7	(0,0)
CS	$J = 2 \rightarrow 1$	97980.9500	IRAM-30m	0.06	270	25	0.76	<0.11	2×2
	$J = 5 \rightarrow 4$	244935.6435	IRAM-30m	1.22	500	10	0.49	<0.4	(0,0)
CCS	$J_N = 2_1 \rightarrow 1_0$	22344.0330	Robledo-70m	0.05	60	41	0.38	<0.5	(0,0)
NH ₃	(J,K)=(1,1)	23694.4955	Robledo-70m	0.50	90	39	0.35	<0.14	1.7×1.7

^aVelocity resolution for each transition.

^bTypical system temperature.

^cHalf power beam width of the telescope.

^dMain beam efficiency.

^ePeak main beam brightness temperature of the line. Uncertainties are 2σ . Upper limits are 3σ .

^fArea over which data were averaged to obtain the quoted T_{MB} , centered on IRAS 16277–2332 for CB 65 and on IRAS 17503–0833 for CB 101. (0,0) means that only the central spectrum was used.

^gLine width at half maximum, obtained from a Gaussian fit to the line. Uncertainties are 2σ , and represent the error in the Gaussian fit.

^hVelocity integrated mean brightness temperature of the line. Uncertainties are 2σ .

Table 4. Infrared data for IRAS 17503–0833

λ (μm)	Flux density (Jy)
1.25	0.48
1.65	0.82
2.17	0.82
12	0.42
25	<0.28
60	<0.42